



# Liquid assisted plasma enhanced chemical vapour deposition with a non-thermal plasma jet at atmospheric pressure

Jan Schäfer<sup>a,\*</sup>, Katja Fricke<sup>a</sup>, Filip Mika<sup>b</sup>, Zuzana Pokorná<sup>b</sup>, Lenka Zajíčková<sup>c,d</sup>, Rüdiger Foest<sup>a</sup>

<sup>a</sup> Leibniz Institute for Plasma Science and Technology e.V., Felix-Hausdorff-Str. 2, 17489 Greifswald, Germany

<sup>b</sup> Institute of Scientific Instruments of the CAS, v.v.i, Královopolská 147, 612 64 Brno, Czech Republic

<sup>c</sup> CEITEC - Central European Institute of Technology, Masaryk University, Kamenice 753/5, 62500 Brno, Czech Republic

<sup>d</sup> Dept. Phys. Electronics, Faculty of Science, Masaryk University, Kotlářská 2, 61137 Brno, Czech Republic

## ARTICLE INFO

### Article history:

Received 26 May 2016

Received in revised form 9 September 2016

Accepted 13 September 2016

Available online 14 September 2016

### Keywords:

Plasma jet

Liquid assisted plasma enhanced chemical vapour deposition

Silicon oxide

Hexamethyldisiloxane

Octamethyltetrasiloxane

Tetrakis(trimethylsilyloxy)silane

## ABSTRACT

The present study introduces a process for the synthesis of functional films onto substrates directly from the liquid phase. The reported method is based on the initialization of the synthesis by means of an atmospheric pressure plasma jet operating with argon above a thin liquid film of the starting material. The process is demonstrated by the formation of a thin, solid SiO<sub>x</sub> film from siloxane-based liquid precursors. Changes in the chemical properties of the precursor were studied in-situ during the polymerization process on the diamond crystal by using Fourier transform infrared spectroscopy. The elemental composition of the SiO<sub>x</sub>C<sub>y</sub> films was analyzed by X-ray photoelectron spectroscopy (XPS). Furthermore, XPS was applied to study the effect of post-annealing processes on the composition of the films. The obtained deposits exhibit a low concentration of carbon groups. The amount of hydroxyl groups and interstitial water can be reduced significantly by post-process annealing of the films.

© 2016 The Author(s). Published by Elsevier B.V. This is an open access article under the CC BY-NC-ND license (<http://creativecommons.org/licenses/by-nc-nd/4.0/>).

## 1. Introduction

The preparation of thin functional films using chemical vapour deposition (CVD) has been established as one of the standard coating technologies today. This method allows the formation of various thin films differentiated by their chemical composition, resulting in diverse chemical, mechanical, optical and electrical properties. CVD is described by heterogeneous chemical reactions of gaseous reactants at the surface leading to formation of solid films on the substrate [1]. If the gas mixture is activated using plasma, this process is called plasma assisted or plasma enhanced chemical vapour deposition (PACVD or PECVD). An essential advantage of PECVD with respect to CVD is the lower substrate temperature and hence the minimized thermal stress of substrates. The application of atmospheric pressure CVD technology has been demonstrated on the industrial scale already in 1969 [2]. However, PECVD processes were until recently dominated by vacuum technologies because suitable plasma sources have been available predominantly for low pressure processing. Several publications dealing with atmospheric pressure PECVD appeared in early investigations of dielectric barrier discharges for plasma polymerization from 1979 onwards [3,4]. Later, non-thermal plasma jets [5,6] served as plasma sources for thin film deposition experiments, e.g. [7,8]. However, despite recent progress

regarding film homogeneity and chemical composition under atmospheric pressure conditions, e.g. from [9,10], it is generally supposed that low pressure methods yield films with superior qualities (e.g. spatial morphological homogeneity). This is attributed to several reasons of intrinsic and of technological nature. Whereas the latter are linked merely to their technological maturity level, the former are related to plasma physical constraints that may have a negative influence on the film properties. We name here e.g. (i) the steep spatial parameter gradients observed in most filamentary discharges which may translate into spatially inhomogeneous film chemistry or (ii) the absence of a steady flux of kinetic (ionic) species to the growing film which plays an essential role in many low pressure PECVD processes by contributing to the formation of denser and pinhole-free films [11]. O'Neill et al. propose a route to barrier coatings using atmospheric pressure plasma liquid deposition in which precursors are introduced into the plasma using an ultrasonic nozzle atomizer [12]. It enables atmospheric pressure PECVD also for liquid precursors with vapour pressures insufficient for evaporation.

There exist several other techniques for the deposition of films operating with liquids. Wet chemistry for surface treatment in general represents a well-established field that is related to the long history which the polymer chemistry has been writing already for more than 100 years [13]. In chemical solution deposition methods, the solution is transferred onto substrates by spin, dip, and spray coating. Its curing and cross-linking are initiated by subsequent exposure to thermal

\* Corresponding author.

E-mail address: [j.schaefer@inp-greifswald.de](mailto:j.schaefer@inp-greifswald.de) (J. Schäfer).

energy, vacuum ultraviolet radiation [14,15] or plasma [16]. The latter process is known as plasma-induced polymerization [17]. Several methods employ the electric field to disperse and/or transport a liquid to be processed, e.g. electrospray or electrospinning, and they can be combined with plasma techniques [18,19,20].

Numerous approaches exist towards the plasma treatment of liquids for the synthesis of materials within the solution. However, to our knowledge, the synthesis of a compact solid thin film which exhibits a stoichiometry close to  $\text{SiO}_2$  by direct plasma treatment of an organosilicon liquid has not been published yet. Therefore, efforts have been made to develop promising approaches for deposition processes at atmospheric pressure. In this study we present a method for the production of thin solid films from the liquid phase referred to as liquid assisted PECVD (LA-PECVD) which is particularly suited for materials with low vapour pressure that are difficult to transfer into the gas phase and furthermore, it facilitates using mixtures of different raw materials.

For the pilot study here, we demonstrate LA-PECVD by comparing three liquid compounds, hexamethyldisiloxane (HMDSO), octamethyltetrasiloxane (OMCTS), and tetrakis(trimethylsilyloxy)silane (TTMS), that are approved precursors for the formation of organosilicon films using PECVD. Indeed, molecular properties of HMDSO have been described already in 1950 [21]. The compound has been used in coating technology for more than 40 years [22]. The usage of OMCTS for PECVD dates back to 1992 and was motivated by demands for improved chemical functionality [23]. According to our recent results, the distinguished steric molecular structure of TTMS offers prospects for the deposition of thin films based on these structures [24].

## 2. Experimental part

### 2.1. Plasma source

The experiments were conducted using the cold atmospheric pressure plasma jet kINPen 11 (neoplas tools, Greifswald, Germany). The plasma jet consists of a high-voltage (HV) needle electrode centred inside a ceramic capillary ( $\varnothing$  1.6 mm) and a grounded outer ring electrode [25]. The central electrode is powered with 2 W at a frequency of 1.1 MHz in this study. The operating rare gas or gas mixture flows through the ceramic capillary. The scheme of the source with experimental conditions is shown in Fig. 1.

### 2.2. Materials

The experiments in this study have been performed using three liquid organosilicon compounds: HMDSO, OMCTS and TTMS (delivered by

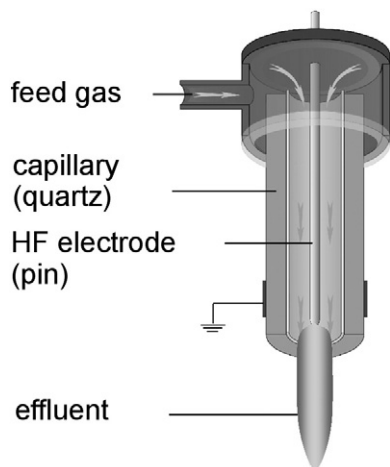


Fig. 1. Plasma source: atmospheric pressure plasma jet kINPen 11 (neoplas tools GmbH) operating at 1.1 MHz, power 2 W, argon flow rate 4.7 slm.

Sigma-Aldrich Chemie GmbH, Germany, purity 98%). The specification of the compounds is given in Table 1. The same amount of HMDSO and OMCTS liquid ( $V_p = 100 \mu\text{l}$ ) was prepared on a circular area  $S = 26 \text{ mm}^2$  on the substrate. It resulted in a droplet height of 3.8 mm. For the TTMS the amount was smaller ( $60 \mu\text{l}$ ) because of lower evaporation losses compared to the aforementioned liquids. The corresponding droplet height was 2.3 mm.

A polished diamond crystal of the attenuated total reflectance Fourier transform infrared (ATR-FTIR) spectrometer (Spectrum One, Bruker) was used as the substrate for the in situ monitoring of material changes and a double-sided polished silicon wafer (thickness 0.2 mm) was used for the comparative ex situ analyses. The plasma source was operated with argon (Linde, purity 5.0) at 4.7 slm.

### 2.3. Process: liquid assisted PECVD (LA-PECVD)

The material synthesis in form of thin solid films proposed here combines the principles of wet-chemical polymerization with plasma enhanced chemical vapour deposition (PECVD). The main difference of LA-PECVD to traditional PECVD is the temporal separation of the coating process into two consecutive steps, which enables to initiate additional chemical reactions. In the first step the precursor liquid is applied to the surface to be coated. In the second step synthesis of the liquid film occurs by exposing the prepared surface to the plasma jet. The interaction of the plasma effluent above the liquid surface adopts characteristics from PECVD, where the active species generated by the jet react with the organic substances. In the case of LA-PECVD additional reactions develop below the liquid – plasma interface and contribute to a more complex material synthesis. The amount of reacting precursor molecules is defined by preparation of the liquid film in the first step.

During the second step, the synthesis of solid products consumes the precursor molecules. In parallel, light volatile molecules evaporate and are in part redeposited back on the surface where they form a solid film material in a process similar to PECVD. An important mechanism of step two relates to the polarisation of the liquid layer by charging of the liquid surface by plasma. This represents also a substantial difference of LA-PECVD to those seemingly similar CVD processes where the liquid raw material is supplied by continuous spraying and its transport to the surface is assisted by means of discharges or applied electric fields (e.g. electrospraying [18]). In particular, during LA-PECVD, the established electric field in the liquid film wetting the substrate contributes to a higher efficiency of the solidification process and hence a higher film production yield. The sequential procedure of LA-PECVD consolidates the effect: at the beginning, the interface substrate – liquid conserves the initial neutral charge and only after the discharge is ignited, the additional electric charge polarises the liquid film and accelerates the mechanisms of LA-PECVD.

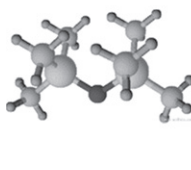
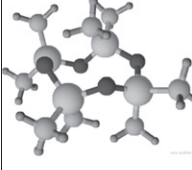
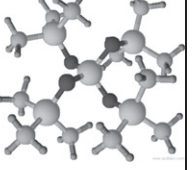
After completion of step two, the process can be repeated in order to achieve the desired film thickness. The methodology of LA-PECVD is shown in Fig. 2 and the process conditions are summarized in the figure caption. For films polymerized from OMCTS and TTMS the ‘plasma ON’ time was 5 min per cycle. Due to the higher vapour pressure of HMDSO, 10 cycles with the ‘plasma ON’ time of 10 min were needed to obtain the coating appropriate for the purpose of surface diagnostics. For the analytical purpose, the films were deposited on silicon wafers at normal laboratory environmental conditions: 30% humidity, 25 °C.

### 2.4. Methods

A complex film analysis that couples a number of complementary surface diagnostics methods allows drawing more profound conclusions with regard to film deposition processes. The chemical surface composition was determined by high-resolution scanning X-ray photoelectron spectroscopy (XPS) using the Axis DLD electron spectrometer (Kratos Analytical, Manchester, UK) with a monochromatic  $\text{Al K}\alpha$

**Table 1**

Overview of liquid organosilicon compounds used in this study. C\* is the atomic percentage of carbon without consideration of H (XPS), [O]/[Si] is the oxygen-to-silicon ratio in the molecule and  $M_r$  is the molecular weight. \*\* values at 25 °C, vapour pressure of TTMS ( $p_r$ ) is taken as a reference value for the comparison with the others liquids.

	HMDSO	OMCTS	TTMS
Structure			
	$C_6H_{18}OSi_2$	$C_{18}H_{24}O_4Si_4$	$C_{12}H_{36}O_4Si_5$
C* [at.%]	67	50	57
[O]/[Si]	0.5	1.0	1.25
$M_r$	162.38	296.62	384.85
Vapour pressure **	56.3 hPa (628× $p_r$ )	125 hPa (14× $p_r$ )	8.96 hPa ( $p_r$ )

source (1486 eV). Charge neutralization was implemented by low energy electron injection into the magnetic field of the lens from a filament located directly atop the sample. The spectra were acquired using medium magnification lens mode and an analysis area of approximately 250  $\mu\text{m}$  in diameter by selecting the slot aperture. Survey spectra and core level spectra of all identified elements were collected at the pass energy of 80 eV whereas the pass energy was set to 10 eV for the highly resolved oxygen (O 1s), carbon (C 1s), and silicon (Si 2p) peaks. Data acquisition and processing were carried out using CasaXPS software, version 2.14dev29 (Casa Software Ltd., Teignmouth, UK). Concentrations are given in XPS atomic percentage (at.%). For the heating experiments, the samples were mounted on a sample holder with a heater and thermocouple directly below. The sample was gradually (increment of 50 °C) heated in situ under ultra high vacuum conditions to temperatures up to 550 °C. The temperature was kept constant for 15 min before the XPS spectra were acquired.

Atomic force microscopy (AFM) was performed using the scanning probe microscope diCP-II (Veeco Instruments, Santa Barbara, CA, USA) in contact mode. An area of 5  $\mu\text{m} \times 5 \mu\text{m}$  was scanned at a scan rate of 0.4 Hz using a silicon probe with aluminium reflective coating (Bruker Axs, MPP-31120, Champs sur Marne, France) with a typical spring constant of about 0.9  $\text{N} \cdot \text{m}^{-1}$ . AFM images were second order smoothed using the open source software Gwyddion 2.39 [26].

The morphological structure of samples was imaged using the scanning electron microscope (SEM) JSM-7500F (JEOL, Japan). It employs a field emission gun and a secondary electron in-lens detector enabling to perform observation of a specimen at a maximum specified resolution of 1.0 nm. In this study, the microscopy of dielectric samples was performed in Gentle Beam Mode with accelerating voltage between 1.3 and 2 kV, and magnitude from 20,000× to 100,000× without additional metal coating at working distances from 8 to 6 mm.

ATR-FTIR spectroscopy using the Spectrum Spotlight 200 microscope (Perkin Elmer, USA) provided qualitative analysis of chemical binding and composition of the films. In this study, the measurements were carried out in situ using the ATR diamond crystal as the substrate for the deposition by means of LA-PECVD. The spectra were obtained at a spectral resolution of 4  $\mu\text{m}$  in the range between 4000–650  $\text{cm}^{-1}$  using an ATR diamond crystal. For each spectrum, 10 scans were averaged in an accumulation time of 60 s and processed using OriginPro 9.1. These experiments could only be realised because of the poor adhesion of synthesized materials to the inert diamond crystal of the ATR spectrometer. Therefore, the reference spectrum was assumed to remain constant without contaminations by previous depositions. This has been proved after each synthesis on the crystal and after successive cleaning of the surface prior to every experiment.

### 3. Results

The study encompasses more than 30 experiments under variation of the operational parameters. The decisive process parameters are: type of precursor, surface temperature and post processing by vacuum annealing.

#### 3.1. Structure of the coatings

The combination of AFM and SEM was used to investigate the morphologic and topographic characteristics of the synthesized coatings. The film thickness was measured at the ion-polished vertical film cross-sections using SEM. In order to increase the contrast between the silicon wafer and the  $\text{SiO}_x$ -based coating the low-angle back-scattered electron detector of the SEM was used because of its sensitivity to the electron energy emitted by different chemical substances.

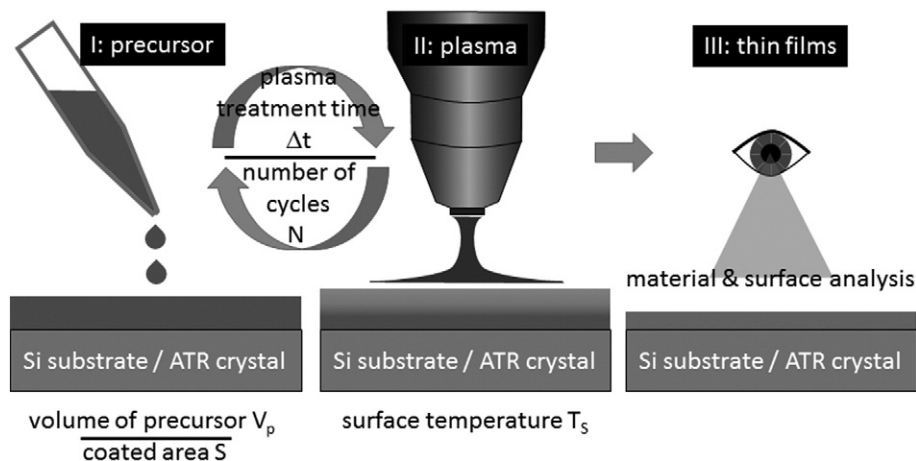


**Fig. 2.** Process steps of liquid assisted PECVD (LA-PECVD). Process parameters: laboratory temperature 25 °C, humidity 30%,  $T_s \approx 25$  °C,  $S = 26 \text{ mm}^2$ , for HMDSO and OMCTS:  $V_p = 100 \mu\text{l}$ ,  $V_p/S = 3.8 \text{ mm}$ , for TTMS  $V_p = 60 \mu\text{l}$ ,  $V_p/S = 2.3 \text{ mm}$ , for HMDSO:  $\Delta t = 10 \text{ min}$ ,  $N = 10$ , for OMCTS and TTMS:  $\Delta t = 5 \text{ min}$ ,  $N = 1$ .

Indeed, the approach enabled to estimate the film thickness with an accuracy better than 5 nm. The polished cross-sections were compared also with manually cleaved substrates to verify that the polishing process caused no artificial changes in the coating. After 10 cycles, a film thickness of 80 nm was obtained from HMDSO, whereas a thickness of 140 nm and 120 nm was obtained after 1 cycle for TTMS and OMCTS, respectively. The relative standard deviation of the thickness measurement was lower than 10%. The vapour pressure of the liquid compounds at 25 °C influences the amount of polymerized material and thus the resulting film thickness, yet the observed proportionality was weaker. Although the vapour pressure of HMDSO is 628 times and that of OMCTS 14 times higher than that of TTMS [27], the average film production yield is in the same order of magnitude: 8 nm/min for HMDSO, 24 nm/min for OMCTS and 28 nm/min for TTMS, based on the specified conditions.

Micrographs of polished cross-sections and manually cleaved samples exhibited a structure typical for a homogeneous amorphous material. However, an additional feature was observed in the cross-section image. The interface layer on the top of the film can be distinguished from the bulk material by means of the low-angle back-scattered electron detector. The thickness of the interface was about 20 nm. Moreover, SEM analysis on top of the coatings revealed a microscopically pitted surface which can be characterized quantitatively by means of AFM. A comparison between SEM histograms and AFM topography analysis for the synthesized films is depicted in Fig. 3. The investigated films were similar regarding the arithmetic mean surface roughness which was found to be in the range 0.3–0.4 nm. Note that the measured roughness of the pristine silicon wafer was 0.1 nm. The OMCTS based coating had a slightly higher surface roughness, 0.43 nm, while for HMDSO and TTMS the values were 0.34 and 0.32 nm, respectively. This result is confirmed by different widths of the AFM distribution profiles in Fig. 3. All profiles can be expressed by a Gaussian distribution which is also the case for the SEM-histograms. For ease of comparison, the SEM images were taken at an observation configuration that extended over the same scanned area as the AFM images. The surface of the TTMS sample seemed to be smooth, without any discernible features as shown by SEM. Moreover, AFM indicated the main surface plane of the TTMS sample at the same height as for the pristine silicon wafer (both at  $z = 1.5$  nm). Furthermore, the SEM micrographs contained broader brightness spectra at the surfaces of HMDSO and OMCTS samples. The width of the SEM histograms is related to a distribution of the topographic inclinations and it indicates laterally larger structures which are significantly higher for HMDSO at 1.8 nm and for OMCTS at 1.7 nm (main surface plane measured by AFM). In order to get a visual impression of the 3D structure, cross-sectional SEM and AFM micrographs were combined. The resulting viewgraph is depicted exemplarily for OMCTS in Fig. 4.

### 3.2. Chemical properties of the coatings

#### 3.2.1. Functional groups

Evidence for the initiation phase of the film synthesis in the liquid was obtained by in situ ATR-FTIR. Changes in the IR spectrum from liquid to solid state are visualized in Fig. 5. Although the molecular structure of the studied liquids is different from each other, the IR spectra of the solid films obtained indicated a similar  $\text{SiO}_x$ -based film structure for all of them. In particular, stretching and bending vibrations of silica with the methyl group in intervals of 1250–1260  $\text{cm}^{-1}$ , 800–840  $\text{cm}^{-1}$ , 754–756  $\text{cm}^{-1}$ , and 686–693  $\text{cm}^{-1}$  were characteristic for the liquid raw compounds and disappeared already after 1 min of plasma treatment. During the polymerization, the main Si-O-Si peak of the asymmetric stretching mode (ASM) at about 1051  $\text{cm}^{-1}$  shifted to higher wavenumbers in the interval of 1065–1069  $\text{cm}^{-1}$ . These two changes demonstrated the oxidation process in the liquid along with losses of carbon groups and with an increased stoichiometry of the  $\text{SiO}_x$  network. Considering the literature on IR spectra of  $\text{SiO}_x$  materials

[28,29,30], the stoichiometry of the synthesized  $\text{SiO}_x$  network can be estimated and it is denoted  $x_{\text{IR}}$ . It was found that  $x_{\text{IR}} = 2.0$  for the films based on HMDSO and TTMS whereas for the film synthesized from OMCTS  $x_{\text{IR}} = 1.9$  was obtained. However, the seemingly high stoichiometric coefficient must be corrected downward considering two additional factors which indicate that the materials differ from pure  $\text{SiO}_2$ . As can be seen in Fig. 5, an intensive peak assigned to Si-OH appears between 920 and 930  $\text{cm}^{-1}$  during the synthesis along with a broad band starting as a left shoulder of the ASM at a wavenumber of 1210  $\text{cm}^{-1}$ . This points towards an incorporation of carbon atoms in the structures, such as  $\text{Si}(\text{CH}_2)_y$ , which contributes to cross-linking of the material. In contrast, the generated hydroxyl groups (detected in the spectra between 2900 and 3700  $\text{cm}^{-1}$ ) do not contribute to the cross-linking, yet, these groups provide hydrogen bridges (3320  $\text{cm}^{-1}$ ) and association with interstitial water (3630  $\text{cm}^{-1}$ ) which in turn can influence the coating properties heavily. Interstitial water can occur in the bulk of the synthesized material as a product of polymerization processes. It is integrated in the molecular network, i.e. as a spacer molecule, and might dictate the nanoporosity of the coating [31].

#### 3.2.2. Material classification

The carbon content and the silicon oxide stoichiometry are two essential parameters for the categorization of  $\text{SiO}_x$ :C films. Because of a large variety of possible structures and interpretations of films with similar chemical compositions, we propose here a classification structure diagram for  $\text{SiO}_x$ :C films based on these two quantities. The diagram is divided into three sections: I. polymers with linear structure, II. cross-linked polymers and III. strongly cross-linked polymers. These sections are defined by prototypical molecular structure units and are summarized in Table 2. The diagram displays the considered structure units whereas their junction lines allow marking the boundaries of corresponding areas as shown in Fig. 6. An important part of section III are inorganic materials (maximum carbon content of 10%) with a stoichiometry close to 2 which is typical for silicon dioxide. Also shown is the classification of the precursors under study. They are characterized as organic liquids with a high concentration of silicon. An interesting classification can be observed for OMCTS which is located at the junction point of polymer-like materials and cross-linked polymers, because of the single ring structure.

The XPS analysis determined both important characteristics of the deposits based on HMDSO (A), OMCTS (B), and TTMS (C): the oxygen-to-silicon ratio (denoted  $x_2$ ) and the carbon content. All of the coatings were chemically similar having the stoichiometry about  $x_2 = 2.3$ , the carbon content of approximately 12 at.% and the silicon percentage below 30 at.%. Deduced from these data, the films are assigned to section II: cross-linked polymers. The relatively high O/Si ratio suggests the presence of a significantly high amount of OH groups (bound to silicon or present in the form of interstitial water) which in turn results in a less cross-linked film. Similar conclusions can be drawn by inspecting the FTIR spectra which confirms the presence of Si-OH functional groups.

#### 3.2.3. Stoichiometry

The assessment of the quality of  $\text{SiO}_x$  network based on the [O]/[Si] ratio provided by the elemental analysis is affected by a significant systematic error because oxygen is not only bridging silicon atoms but also creating OH end-groups, bound with carbon or in water. The caused disproportion can be already demonstrated by comparing the mean XPS elemental ratio [O]/[Si],  $x_2 = 2.3$ , to the stoichiometry obtained from the FTIR spectroscopy ( $x_{\text{IR}} = 1.9$ –2.0). Therefore, we derived the stoichiometry of the  $\text{SiO}_x$  network from highly resolved measured Si 2p XPS spectra. The original and fitted Si 2p peak of the studied films is shown in Fig. 7. Based on the literature it is possible to distinguish between different oxidation degrees of silicon related to the number of bound oxygen atoms  $\text{Si}(-\text{O})_n$ , where  $n \in [1;4]$ , and to quantify the



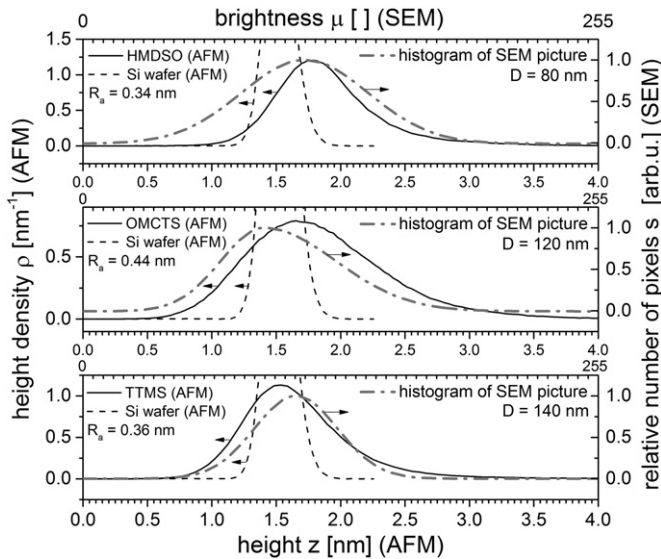


**Fig. 3.** Comparison of height distributions  $\rho(z)$  obtained by AFM (left and bottom coordinates) and brightness histograms  $\mu(s)$  (right and top coordinates) obtained from top view SEM pictures of the films on silicon wafer. Arrows denote the corresponding axis. Arithmetic roughness  $R_a$  (AFM) and film thickness  $D$  obtained from side view SEM pictures is given.

binding percentages  $b_{1,2,3,4}$  of the particular component in the material [32]. The results demonstrate the dominance of the  $\text{Si}(-\text{O})_4$ ,  $b_4$ , component with a percentage between 57 and 59%. The information of binding composition enables the calculation of the stoichiometry,  $x_1$ , as half of the mean oxidation degree  $n/2$  with the following equation:

$$x_1 = n/2 = 2b_4 + 1.5b_3 + b_2 + 0.5b_1 \quad (1)$$

The comparison of the atomic ratio  $x_2 = [\text{O}]/[\text{Si}]$  and the half of the mean oxidation degree  $x_1 = n/2$  is given in Fig. 7, too. Strictly speaking, both approaches for estimating the stoichiometry  $x_{1,2}$  are only equal ( $[\text{O}]/[\text{Si}] = n/2$ ) for chemically homogeneous materials. Taking into account this fact, the quantification of the material inhomogeneity was calculated according to  $\Delta x = x_2 - x_1$ . The stoichiometry  $x_1$ , calculated from the binding composition of Si 2p, is between 1.7 and 1.8 for all deposits which is lower compared to the  $[\text{O}]/[\text{Si}]$  ratio calculated from XPS elemental analysis ( $x_2 = 2.2\text{--}2.4$ ). Therefore, a significant amount of oxygen is not bound to silicon only, but also to carbon or in water. The

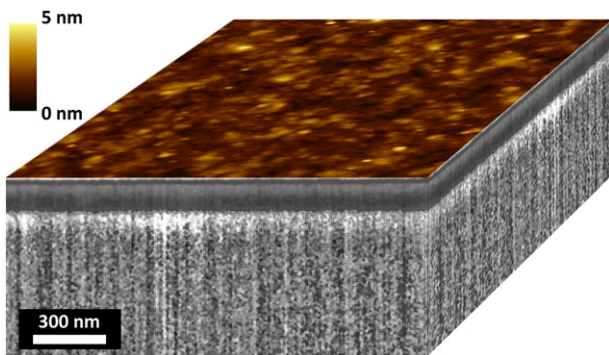


**Fig. 4.** 3D model of the coating by means of LA-PECVD from OMCTS combining vertical cross-sectional SEM and AFM micrographs. The cross-section of the sample has been polished with an argon beam polisher and investigated with the low-angle back-scattered electron detector in order to obtain the maximum material contrast. The analysis revealed the film thickness of 120 nm and an upper interface layer of the film with the thickness of 20 nm. The substrate was silicon wafer.

parameter  $\Delta x$  enables to quantify the amount of oxygen  $\delta[\text{O}]$  which is not bound to silicon by using the following equation:

$$\delta[\text{O}] = \frac{\Delta x}{x_2} = 1 - \frac{2b_4 + 1.5b_3 + b_2 + 0.5b_1}{[\text{O}]/[\text{Si}]} \quad (2)$$

where  $b_{1,2,3,4}$  are the percentages of binding components  $\text{Si}(-\text{O})_{1,2,3,4}$  (see the columns in Table 2). For the coating based on HMDSO, 25% of the total oxygen was not bound to silicon whereas it was 18% for the samples obtained from OMCTS and TTMS. The differences between the coatings A–C suggest that the process based on TTMS produces coatings closest to the section of inorganic materials resembling silicon dioxide, while the coating from HMDSO exhibits the lowest cross-linking degree of the plasma-polymer network with the highest concentration of non-silicon compounds inside.

### 3.2.4. Improvement of the material quality

The incorporation of water within the materials presents a problem of LA-PECVD in general. In the following, we demonstrate a chemical transformation of the coating with respect to the enhancement of inorganic properties by an annealing process subsequently to the deposition. The post-process heating was conducted in the XPS analysis chamber at temperatures up to 450–550 °C which enables the in situ analysis of the chemical composition. The results are presented in the structure diagram in Fig. 8. The prepared films are located in the region of interest defined by prototypical structural units 1 (pure  $\text{SiO}_2$ ), 2 (cross-polymers  $\text{SiO}_{2.5}$  with hydroxyl groups), and 3 (cross-polymers  $\text{SiO}_{1.5}$  with methyl groups) introduced in Table 2.

The films based on HMDSO (A), OMCTS (B) and TTMS (C) are displayed at the same positions in Fig. 8 as already shown in Fig. 6. Annealing of the samples was conducted one month after the deposition. Therefore, the starting points at 30 °C are shifted from section II to section III indicating a post polymerization process and hence, more cross-linked films. Despite the time effect, the coatings exhibited still a significant difference between the total  $[\text{O}]/[\text{Si}]$  ratio ( $x_2$ ) and the half of the oxidation degree of Si with O ( $x_1$ ) at the beginning of the annealing. As expected, the storage did not lead to a significant reduction of the residual oxygen concentration present mainly in water and, therefore, both the stoichiometric parameters differ. However, already after increasing the temperature from 30 °C to 200 °C we observe a decrease of this difference for all samples indicating the decrease of relative

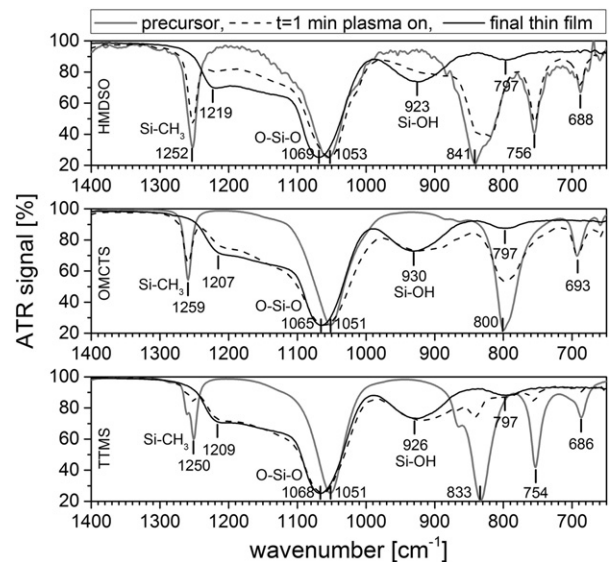


**Fig. 5.** Comparison of ATR spectra of the organosilicon liquids and the synthesized thin films during LA-PECVD. Here, the films were synthesized directly on the diamond ATR crystal in order to observe the instantaneous changes in the film chemistry.

**Table 2**

Model of prototypical molecular structures in  $\text{SiO}_x$ . For the particular units the molecular structure, stoichiometry, O/Si ratio, and carbon percentage are given. \*) for the calculation of percentages no H is considered (XPS).

Prototypical structures in $\text{SiO}_x$ -based materials	unit #			
	1	2	3	10
Inorganic $\text{SiO}_2$ (cross-linked)	2 0			O/Si C [%]*
Cross-polymers	2.5 0		1.5 29	
Polymers (linear chains)	4 3 0		5 2 25	
Monomer groups	7 3.5 0		8 2.5 22	
		9 1.5 44		10 0.5 67
	n=4	n=3	n=2	n=1
	Oxidation degree of silicon in $\text{Si}_2\text{O}_n$			

percentage of oxygen not bound to silicon. This trend is more pronounced with increasing temperature and the stoichiometric parameters  $x_1$  and  $x_2$  converge towards each other. In case of sample A, both the parameters become equal at 450 °C. At this point no difference between the stoichiometry from the global elemental analysis and the binding analysis of Si 2p is observed. The sample A contains no interstitial water, its stoichiometry is close to 1.9 and only a small residuum of 5 at.% carbon has been detected. In case of samples B and C, the crossing point is not reached exactly, however, just 1.4 at.% of oxygen not bound to silicon and about 5 at.% of carbon remained in the materials when a temperature of 550 °C was reached, while the stoichiometry of the materials was found to be approximately 1.8.

Annealing of the prepared films did not cause only the removal of interstitial water. In the structure diagram it is shown that the lower estimate of the stoichiometry based on the binding analysis increases during the annealing along with the boundaries of section III for all

the samples. This line is defined as a junction line between the structure units 3 and 1 (see Table 2). Therefore, the change from 3 towards 1 can be interpreted as a removal of residual methyl groups and their replacement with residual oxygen in the strongly cross-linked plasma polymer.

## 4. Discussion

### 4.1. Growth rate

When optimizing LA-PECVD the specific physical properties of the applied liquids – particularly their vapour pressures – need to be considered. Here, the tuning of the process parameters was motivated by the necessity to obtain a comparable film thickness, about 100 nm, for analytical purposes. The synthesis from HMDSO occurred in 10 cycles during 10 min (8 nm per cycle, 1 cycle = 1 min 'plasma ON') while the other processes were finished after the 'plasma ON' time of 5 min within 1 cycle (120–140 nm). Additionally, the initial amount of liquid was 100  $\mu\text{l}$  for HMDSO and OMCTS (thickness of liquid film 3.8 mm), respectively, and only 60  $\mu\text{l}$  for TTMS (2.3 mm). The process optimisation allowed driving the synthesis by LA-PECVD with liquids of vapour pressure up to 56 hPa. If a surface temperature control is implemented liquids with higher vapour pressures can be applied, too.

In the study we characterized the film growth by averaged values of the deposition rate or by the yield. However, the temporal dependency of the growth rate might differ from the corresponding mean value. In particular, the upper interface between the plasma and liquid is established at the beginning of the process step two. The qualitative changes in the liquid have been detected by means of in situ ATR after 60 s of the process time. Regarding the sensitivity of the ATR spectrometer, small chemical changes can be detected up to a depth of several microns for this time. The evidence of the interface has been demonstrated by cross-sectional SEM pictures after deposition (Fig. 4). The thickness of the interface (about 20 nm) is related to the interaction depth of the plasma. Recent live science investigations of the surface interactions between plasma and water reveal that a penetration depth between several microns and 1 mm is established after 60 s depending on the chemical species [33].

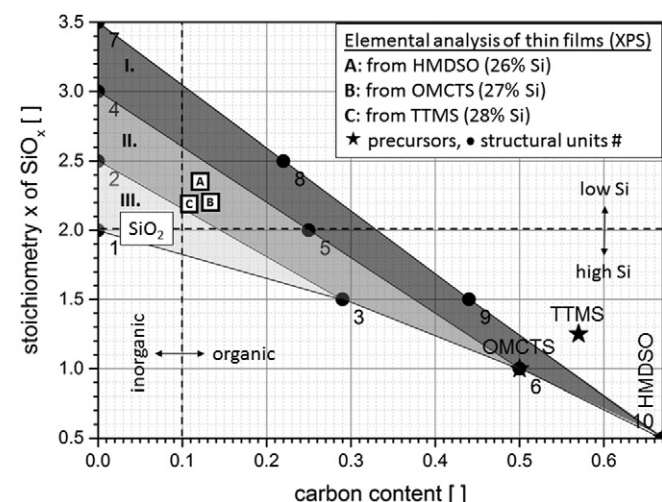


**Fig. 6.** Structure diagram for the classification of organosilicon materials. The particular structural units labelled by numbers 1–10 are specified in Table 2. The positions of the samples A, B and C in the diagram correspond to XPS analyses shortly after the film synthesis. The original liquid compounds, HMDSO, OMCTS and TTMS, used for the synthesis are located in the organic part of diagram with a high carbon and silicon concentration.

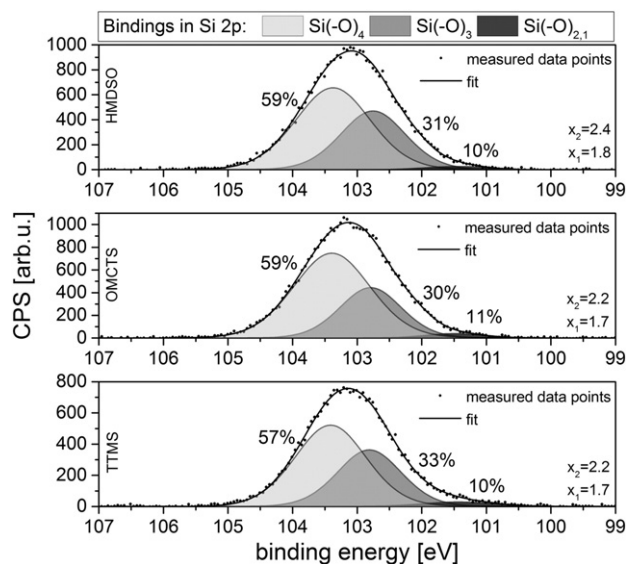


**Fig. 7.** Comparison of binding analysis of XPS Si 2p peaks. The calculation of the  $\text{SiO}_x$  network stoichiometry resulting from the elemental analysis ( $x_2 = [\text{O}]/[\text{Si}]$ ) and from the binding analysis ( $x_1 = n/2$ , where  $n$  is the mean oxidation degree) is given for all the films, too. Areas below the fits of particular components  $\text{Si}(-\text{O})_{1-4}$  determine the corresponding percentage  $b_{1-4}$  of the components considered in Eqs. (1) and (2). The analysis displays the situation shortly after deposition.

## 4.2. Structure model

The use of the proposed structure diagram in Fig. 6 enables a robust classification of the compiled results achieved by FTIR and XPS. Note that a lot of more complicated structural units are not necessarily considered for the definition of the areas as assumed in Table 2. However, the definition of the diagram allows to use it also for studies on more complex structures of organosilicon compounds. We used the diagram in order to show material changes during processes, and additionally to demonstrate their capability to produce homogeneous, analytically distinct material. Annealing up to temperatures as high as 550 °C was applied primarily for methodologic purpose. Of course most practical applications of LA-PECVD would be limited to lower temperatures due to the thermal instability of most substrate materials with relevance to this process, and also because of safety regulations regarding the handling of organosilicon compounds.

## 5. Conclusion

With this study we demonstrate that an atmospheric pressure plasma jet (kINPen) operating at low electric power (<2 W) can be effectively applied as a source of energy and active species for the initiation of chemical synthesis in liquid organosilicon compounds. SiO<sub>x</sub> coatings with a small amount of carbon were synthesized from three liquid organosilicon compounds, HMDSO, OMCTS and TTMS. We also present the approach combining results from SEM and AFM into one overall visualisation of the film morphology/topography and the methodology to combine results from in situ ATR-FTIR and ex situ XPS to obtain a more complex picture of the film chemical structure. Furthermore, the chemical structure could be elucidated using XPS applied in situ during post-process vacuum annealing of the films.

For the general characterisation of the chemical properties of organosilicon materials we propose a structural diagram wherein the structure and their modification can be described. The film materials prepared by LA-PECVD from different organosilicon compounds are surprisingly similar regarding the chemical properties. They can be classified as cross-linked SiO<sub>x</sub> plasma polymers with a high content of hydroxyl groups and interstitial water, while the carbon content was below 15 at.% and the stoichiometry was roughly about  $x = 2$  depending on the diagnostics method. The stability of the molecular network was sufficient for a continuous internal polymerization after the plasma

process. Additional enhancement of the inorganic properties of the coatings was achieved by a thermal acceleration of the cross-linking and parallel exclusion of the interstitial water at temperatures over 200 °C. Samples annealed up to 500 °C exhibited properties similar to silicon dioxide with a remarkable low carbon and water content below 5 at.% and 1 at.%, respectively. The surface of all deposits exhibits an extremely low roughness of about 0.4 nm and the stoichiometric interval  $[x_1, x_2]$  was stabilised at 1.80–1.85 ( $\Delta x = 0.05$ ). With these results, the synthesized material is fully comparable to coatings obtained from conventional PECVD.

The main advantage of LA-PECVD consists in the operation with colloids or liquids which have a lower vapour pressure than needed for the vapour transport in PECVD set-ups. In the present study, this was particularly the case for OMCTS and TTMS. By using TTMS it is possible to achieve an average film production yield of 28 nm/s, which is three times higher than that of HMDSO and about one to two orders of magnitude higher than the growth rate in a PECVD of SiO<sub>x</sub> films at atmospheric pressure [34] or low pressure [35]. Despite the high yield, the surface roughness of the coating deposited from TTMS remained low, 0.36 nm. Nevertheless, one drawback is the need of a post treatment, e.g. annealing, to improve the film properties because of the relatively high content of interstitial water initially incorporated in the films. However, another essential advantage of LA-PECVD is the prospect of mixing the liquid raw substances, in order to adjust the microscopic structure of the synthesized materials and their chemical properties. Moreover, the technique of LA-PECVD can be applied also for colloids, e.g. organosilicon liquids with dispersed nanoparticles. Hence, LA-PECVD is a promising method which provides new possibilities for a number of different applications in thin film technology.

## Acknowledgments

The work has been funded in part by the following sources: 7th European Framework Program, project no. 316216, "PlasmaShape"; DFG, Transregio 24 "Fundamentals of Complex Plasmas"; project CAS (RVO:68081731), by the Ministry of Education, Youth and Sports of the Czech Republic (MEYS CR) under the project CEITEC 2020 (LQ1601) and by MEYS CR under the project LO1212, its infrastructure by MEYS CR and EC (CZ.1.05/2.1.00/01.0017).

## References

- [1] R. Foest, M. Schmidt, H. Gargouri, Self-assembling and self-limiting monolayer deposition, *Eur. Phys. J. D* 68 (2014) 23.
- [2] L.A.B. Pilkington, Float glass process, *Proc. R. Soc. Lond. A* 314 (1969) 1–25.
- [3] K.G. Donohoe, T. Wydeven, Plasma polymerization of ethylene in an atmospheric pressure discharge, in: S. Veprek, J. Hertz (Eds.), *Plasma Chemistry (ISPC-4)*, Zürich, 27.8-1.9.1979 1979, pp. 765–771.
- [4] S. Kanazawa, M. Kogoma, T. Moriawaki, S. Okazaki, Stable glow plasma at atmospheric pressure, *J. Phys. D. Appl. Phys.* 21 (1988) 838–840.
- [5] H. Koinuma, H. Ohkubo, T. Hashimoto, K. Inomata, T. Shiraishi, A. Miyana, S. Hayashi, Development and application of a microbeam plasma generator, *Appl. Phys. Lett.* 60 (7) (1992) 816–817.
- [6] M. Klíma, L. Zajíčková, J. Janča, The perspectives of plasmachemical treatment on ancient artifacts, *Z. Schweiz. Archäol. Kunstgesch.* 54 (1997) 31–33.
- [7] V. Raballand, J. Benedikt, A. von Keudelt, Deposition of carbon-free silicon dioxide from pure hexamethyldisiloxane using an atmospheric microplasma jet, *Appl. Phys. Lett.* 92 (2008) 091502.
- [8] J. Schäfer, R. Foest, A. Quade, A. Ohl, J. Meichsner, K.-D. Weltmann, Carbon-free SiO<sub>x</sub> films deposited from octamethylcyclotetrasiloxane (OMCTS) by an atmospheric pressure plasma jet (APJ), *Eur. Phys. J. D* 54 (2009) 211–2017.
- [9] D. Trunc, L. Zajíčková, V. Buršíková, F. Studnička, P. St'ahel, V. Prysiazhnyi, V. Peřina, J. Houdková, Z. Navrátil, D. Franta, Deposition of hard thin films from HMDSO in atmospheric pressure dielectric barrier discharge, *J. Phys. D. Appl. Phys.* 43 (2010) 225403.
- [10] S.A. Starostin, P. Antony Premkumar, M. Creatore, H. de Vries, R.M.J. Paffen, M.C.M. van de Sanden, High current diffuse dielectric barrier discharge in atmospheric pressure air for the deposition of thin silica-like films, *Appl. Phys. Lett.* 96 (2010) 061502.
- [11] E.V. Johnson, S. Pouliquen, P.A. Delattre, J.P. Booth, Hydrogenated microcrystalline silicon thin films deposited by RF-PECVD under low ion bombardment energy using voltage waveform tailoring, *J. Non-Cryst. Solids* 358 (17) (2012) 1974–1977.

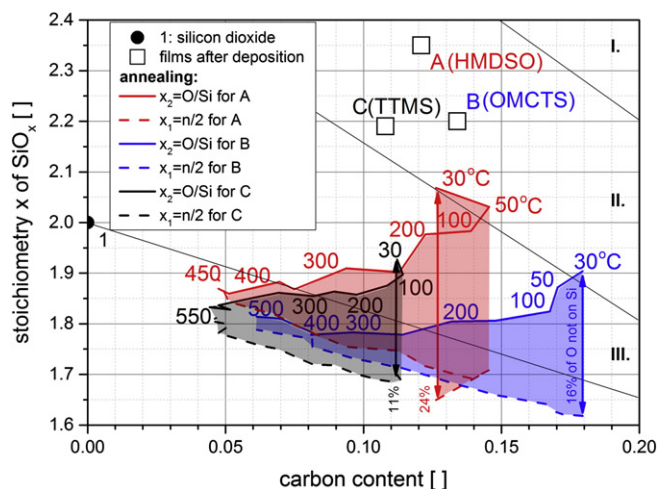


Fig. 8. Dynamic changes of the films during their vacuum annealing up to 550 °C presented in the structure diagram as in Fig. 6. The coefficients  $x_{1,2}$  denote different views on the stoichiometry of SiO<sub>x</sub> network,  $n$  is the mean oxidation degree defined by Eq. (1). The difference between the characteristics (coloured areas) demonstrates the chemical homogenisation of the films with temperature. The percentage of oxygen atoms not bound to silicon is calculated at the initial annealing temperature for all the films by Eq. (2).



- [12] L. O'Neill, L.-N. O'Hare, S.R. Leadley, A.J. Goodwin, Atmospheric pressure plasma liquid deposition – a novel route to barrier coatings, *Chem. Vap. Depos.* 11 (2005) 477–479.
- [13] H. Staudinger, Über polymerisation, *Ber. Dtsch. Chem. Ges.* 53 (1920) 1073–1085.
- [14] C. Dölle, M. Pappmeyer, M. Ott, K. Vissing, Gradual photochemical-induced conversion of liquid polydimethylsiloxane layers to carbon containing silica coatings by VUV irradiation at 172 nm, *Langmuir* 25 (12) (2009) 7129–7134.
- [15] P. Swiderek, E. Jolondz, J.H. Bredeho, T. Borrmann, C. Dölle, M. Ott, C. Schmüser, A. Hartwig, V. Danilov, H.-E. Wagner, J. Meichsner, Modification of polydimethylsiloxane coatings by H<sub>2</sub> RF plasma, Xe<sub>2</sub>\* excimer VUV radiation, and low-energy electron beams, *Macromol. Mater. Eng.* 297 (11) (2012) 1091–1101.
- [16] J. Schäfer, Complex Condensation of Ethylene Glycol in an RF Low Pressure Plasma (PhD Thesis) University of Greifswald, 2007.
- [17] F. Epailard, J.C. Brosse, G. Legeay, Plasma-induced polymerization, *J. Appl. Polym. Sci.* 38 (1989) 887–898.
- [18] J. Friedrich, R. Mix, R.D. Schulze, A. Rau, Ultra-thin polymer layer deposition by aerosol-dielectric barrier discharge (DBD) and electro-spray ionization (ESI) at atmospheric pressure, *J. Adhes. Sci. Technol.* 24 (7) (2010) 1329–1350.
- [19] A. Manakhov, D. Nečas, J. Čechal, D. Pavliňák, M. Eliáš, L. Zajíčková, Deposition of stable amine coating onto polycaprolactone nanofibers by low pressure cyclopropylamine plasma polymerization, *Thin Solid Films* 581 (2015) 7–13.
- [20] D. Pavlinak, J. Hnilica, A. Quade, J. Schäfer, M. Alberti, V. Kudrle, Functionalisation and pore size control of electrospun PA6 nanofibres using a microwave jet plasma, *Polym. Degrad. Stab.* 108 (2014) 48–55.
- [21] K. Yamasaki, A. Kotera, M. Yokoi, Y. Ueda, An electron diffraction study of structures of tetramethylorthosilicate, hexamethyldisiloxane, and hexachlorodisiloxane, *J. Chem. Phys.* 18 (1950) 1414–1415.
- [22] Y. Segui, B. Ai, Gas discharge in hexamethyldisiloxane, *J. Appl. Polym. Sci.* 20 (1976) 1611–1618.
- [23] J. Janča, L. Sodomka, Selective gas sorption of plasma-polymerized organosiloxane thin films, *Thin Solid Films* 216 (1992) 235–238.
- [24] J. Schäfer, J. Hnilica, J. Šperka, A. Quade, V. Kudrle, R. Foest, J. Vodák, L. Zajíčková, Tetrakis(trimethylsilyloxy)silane for nanostructured SiO<sub>2</sub>-like films deposited by PECVD at atmospheric pressure, *Surf. Coat. Technol.* 295 (2016) 112–118.
- [25] K.D. Weltmann, E. Kindel, R. Brandenburg, C. Meyer, R. Bussiahn, C. Wilke, T. von Woedtko, Atmospheric pressure plasma jet for medical therapy: plasma parameters and risk estimation, *Contrib. Plasma Phys.* 49 (9) (2009) 631–640.
- [26] D. Nečas, P. Klapetek, Gwyddion: an open-source software for SPM data analysis, *Cent. Eur. J. Phys.* 10 (1) (2012) 181–188.
- [27] Y.D. Lei, F. Wania, D. Mathers, Temperature-dependent vapor pressure of selected cyclic and linear polydimethylsiloxane oligomers, *J. Chem. Eng. Data* 55 (2010) 5868–5873.
- [28] P.G. Pai, S.S. Chao, Y. Takagi, G. Lucovsky, Infrared spectroscopic study of SiO<sub>x</sub> films produced by plasma enhanced chemical vapor deposition, *J. Vac. Sci. Technol. A* 4 (1986) 689–694.
- [29] W. Kaiser, P.H. Keck, C.F. Lange, Infrared absorption and oxygen content in silicon and germanium, *Phys. Rev.* 101 (1956) 1264.
- [30] J. Schäfer, R. Foest, A. Quade, A. Ohl, K.-D. Weltmann, Local deposition of SiO<sub>x</sub> plasma polymer films by a miniaturized atmospheric pressure plasma jet (APPJ), *J. Phys. D: Appl. Phys.* 41 (2008) 194010.
- [31] A. Perrotta, E.R.J. van Beekum, G. Aresta, A. Jagia, W. Keuning, R.M.C.M. van de Sanden, E.W.M.M. Kessels, M. Creatore, On the role of nanoporosity in controlling the performance of moisture permeation barrier layers, *Microporous Mesoporous Mater.* 188 (2014) 163–171.
- [32] M.R. Alexander, R.D. Short, F.R. Jones, W. Michaeli, C.J. Blomfield, A study of HMDSO/O<sub>2</sub> plasma deposits using a high-sensitivity and -energy resolution XPS instrument: curve fitting of the Si 2p core level, *Appl. Surf. Sci.* 137 (1999) 179–183.
- [33] C. Chen, D.X. Liu, Z.C. Liu, A.J. Yang, H.L. Chen, G. Shama, M.G. Kong, A model of plasma-biofilm and plasma-tissue interactions at ambient pressure, *Plasma Chem. Plasma Process.* 34 (2014) 403–441.
- [34] J. Schäfer, R. Foest, F. Sigener, D. Loffhagen, K.-D. Weltmann, U. Martens, R. Hippler, Study of thin film formation from silicon-containing precursors produced by an RF non-thermal plasma jet at atmospheric pressure, *Contrib. Plasma Phys.* 52 (10) (2012) 872–880.
- [35] M.I. Alayo, I. Pereyra, M.N.P. Carreno, Thick SiO<sub>x</sub>N<sub>y</sub> and SiO<sub>2</sub> films obtained by PECVD technique at low temperatures, *Thin Solid Films* 332 (1998) 40–45.